Imaging Life

Biological Systems from Atoms to Tissues

EDITED BY GARY C. HOWARD

WILLIAM E. BROWN

AND

MANFRED AUER

9

Breaking Abbe's Law

Super-Accuracy and Super-Resolution Fluorescence Microscopy based on Single Molecule Detection

SETHURAMASUNDARAM PITCHIAYA,
JOHN R. ANDROSAVICH, AND NILS G. WALTER ■

INTRODUCTION

The cell is a complex mixture of single molecules that function in a highly organized and concerted manner to forge life. Conversely, each molecule within the cell is, in principle, a local reporter on the nature and dynamics of its surroundings. Yet studies of biomolecules, such as probing their structure, measuring their reaction kinetics, or determining their intracellular distribution, have mostly been conducted on the ensemble level, reporting the "average" structure, mechanism, or cellular organization. Important information is hidden within this average, as a seemingly homogenous population of molecules can, in fact, be composed of surprising heterogeneity. In addition, the flow of genetic information is spatially and temporally organized through the transport of single mRNA molecules to discrete regions in an organ (1) or even a single cell (2, 3) to synthesize proteins in the region where they are needed most. For example, as seen by live-cell fluorescence microscopy, a significant fraction of the mRNA encoding the cytoskeletal protein actin localizes to the leading edge of the cell. Upon tracking the diffusion of single actin mRNA molecules, multidirectional movements with net displacement vectors pointing towards the leading edge of the cell were observed, thus rationalizing the average cellular organization of the mRNA (4).

Single-molecule fluorescence microscopy (SMFM) generally reveals rare events and transient species or intermediates on a reaction pathway, like those found in protein (5, 6) or RNA folding landscapes (7, 8), without the need to perturb or synchronize the molecules of the system to generate a signal. Such information is easily lost by averaging in regular ensemble measurements. According to the ergodic theorem, the time average of any observable obtained from visualizing a single molecule is equivalent to the population average, provided the molecule is visualized over a sufficiently long period of time. Yet, single-molecule studies have also shown that some RNA and protein enzymes exhibit so-called static heterogeneity

with conformationally and functionally distinguishable molecular species that only slowly exchange on an experimental time scale (7, 9–12). The types of information obtained from SMFM thus provide unprecedented insights into the functional mechanisms, dynamic properties, and subcellular localization of biomolecules, with only limited perturbation of the underlying biology.

Two major aspects of microscopy, accuracy and resolution, define the quality of imaging in a quantitative manner. On one hand, accuracy describes the radius of the circle (or sphere in the case of three-dimensional localization) within which it is certain that an object is localized (i.e., the error associated with localizing an object). On the other hand, resolution is the distance below which two closely located objects cannot be distinguished as separated from one another. In 1873 Ernst Abbe observed the failure of a lens-based optical microscope to distinguish two features closer than half of the wavelength of the illumination light on the lateral plane. This imposes a theoretical limit on the resolution of fluorescence microscopy of 200–300 nm (using visible, ~500-nm illumination light). This relationship is more accurately described by:

$$\Delta d = \frac{\lambda}{2n\sin\alpha} \tag{1}$$

where Δd is the distance between two closely located spots, λ is the wavelength of light used for illumination, n is the refractive index of the medium in which the lens is working, and α is the half-angle of the maximum cone of light that enters or exits the lens. The obtainable axial resolution as described by:

$$\Delta z = \frac{\lambda}{2n\sin^2\alpha} \tag{2}$$

is almost threefold higher than the resolution limit in the lateral dimension (~500–600 nm).

For over a century, Abbe's law (also referred to as "Rayleigh's resolution limit") was considered a fundamentally limiting factor in intracellular imaging. This problem is exacerbated for single molecules: their intracellular density is often much higher than that commonly used in SMFM, leading to severe overlap of their images. Given that a typical human cell contains ~10^{10} protein molecules (13) of ~2.5-nm radius and the cell by itself has a volume of ~$4x10^{12}$ nm^3, a conservative estimate of ~20 percent of the total cell volume is filled with just proteins. Factoring in other molecules, such as lipids, nucleic acids, inorganic ions, and small metabolites, the density of molecules, in general, within a cell is astoundingly high. Even in such a crowded environment biomolecules often diffuse at speeds of several nanometers per second, frequently colliding with other molecules and changing direction. Studying single molecules under such conditions necessitates the need for higher accuracy and resolution than that obtained from conventional optical microscopy.

This chapter will provide an overview of the currently available ultra-high-resolution microscopy methods that can be used to visualize single molecules labeled with fluorescent probes in vitro and in vivo (the latter mostly in live cultured cells). These methods can be categorized as: i.) methods pertaining to localization of a few single molecules with nanometer-scale precision (super-accuracy imaging (14)); and ii.)

methods resolving many single molecules within a densely populated sample by localizing only a sparse subset of them at a time through repeated super-accuracy imaging (often termed super-resolution imaging (14)). Other single molecule techniques, such as manipulation by optical tweezers or imaging by atomic force microscopy (AFM), are beyond the scope of this chapter. A detailed description of AFM can be found in an accompanying book chapter and a broad overview of all single-molecule methods can be found in several recent books and reviews (15–17).

EXPERIMENTAL DESIGN IN SINGLE-MOLECULE FLUORESCENCE MICROSCOPY

The sensitivity required to detect single molecules is achieved by carefully selecting the sample concentration, instrumentation, and probe used to label the molecule. The concentration of molecules should be kept low enough, in the nanomolar to picomolar range, to distinguish one molecule from another. While controlling sample concentration in vitro is relatively easy, it presents a major challenge in vivo. Another important parameter to be optimized in SMFM is the signal-to-noise ratio (SNR) (i.e., the ratio of useful signal (photons) emitted by single molecules and unwanted, spurious background signal (noise)). Noise can arise from impurities in the sample, from fluorescent molecules in the sample that are not in focus, or from shot noise (dark counts) of the detector. From its definition, it is clear that having a high SNR is preferred, but several factors can markedly affect this value (as discussed below). A whole arsenal of solutions, in the form of improved optical configurations (illumination methods, light sources, and detectors) and fluorescent probes, is currently available and constantly being refined to overcome low SNR.

MODES OF ILLUMINATION

Schemes to illuminate a sample can be primarily divided into two categories: far-field illumination and near-field illumination. In far-field imaging, the distance between the objective lens and sample is at least an order of magnitude greater than the wavelength of light used. Conversely, in near-field imaging, the sample is separated from the illuminating focusing lens or fiber optics by a distance much smaller than the illumination wavelength. Additionally, the diameter of the lens or fiber is smaller than the wavelength of light used (typically ~80 nm) (18, 19). Such a configuration ensures that the light interacts with the sample before effects of diffraction come into play, leading to higher resolution. Near-field illumination requires very flat samples for the lens or fiber optics to scan over it, making it less useful for intracellular imaging. In the following, we focus on some of the more popular far-field illumination schemes used in SMFM (Figure 9.1).

Wide-Field Epi-Illumination

In wide-field epi-illumination schemes, light passes through the objective's optical axis, illuminating all molecules in the light path. Although a specific plane of the

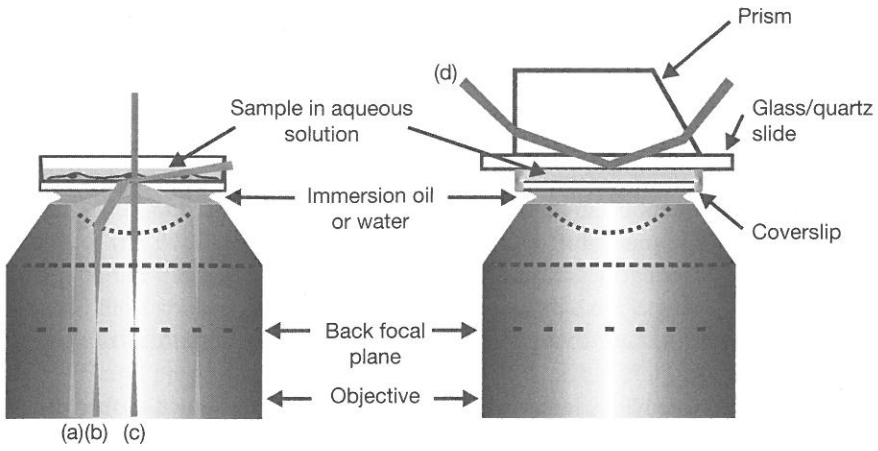

Figure 9.1 Wide-field illumination methods. In live cell imaging, typically, OTIRF (a), HILO (b), or wide-field epi-illumination (c) is used. By simply moving the excitation light away from the optical axis, one can switch from wide-field epi-illumination to HILO or OTIRF. In all three cases, the incident light and the fluorescent light pass through the same objective. By contrast, in PTIRF (d) the incident light is directed to the sample through a prism. The fluorescent light passes through the depth of the sample and the coverslip before being collected by the objective. As the sample has to be sandwiched between the slide and the coverslip, PTIRF is not suitable for live cell imaging, which demands frequent media change and precise control of O_2/CO_2 gas.

sample can be focused, molecules present in other focal planes also get excited, contributing significant background. This illumination method is suitable for SMFM only when bright molecules are sparsely distributed, such that background contribution from out-of-focus molecules is negligible.

Total Internal Reflection (TIR) Illumination

TIR was first used in 1981 by Daniel Axelrod in conjunction with fluorescence (TIR*F*) and fluorescence microscopy (TIR*FM*) to image the lipid probe 3,3′-dioc ta-decyclindocarbocyanine (dil) in human skin fibroblasts (20). When light is transmitted through a medium of higher refractive index (n_i; e.g., glass) into one of lower refractive index (n_r; e.g., water) at incident angles (θ_i) greater than the critical angle given by $\theta_c = \sin^{-1}(n_r/n_i)$ (Snell's Law), light is totally reflected within the first medium. However, because of its wave properties, some light will be transmitted into the medium of lower refractive index in the form of a "standing" or "evanescent" wave. The intensity of this light field decreases exponentially from the interphase, establishing only a thin lamina of ~150-nm depth within the aqueous sample, effectively reducing background fluorescence from outside regions. TIR can be achieved by illumination through either a high numerical aperture (NA) objective (objective-type TIRFM, or OTIRFM) or a quartz prism that couples the incident light into the glass surface (prism-type TIRFM, or PTIRFM). In OTIRFM, the incident laser light is focused onto the back focal plane (BFP) of the objective so that it is away

from and parallel to the optical axis, thus θ_c is achieved without needing an inclined light source. Since the incident light and the fluorescent light are focused by the same objective, scattering of laser light within the objective leads to some background in the image. PTIRFM avoids this background, but poses geometric constraints due to the greater challenge to couple the incident light at the right angle and the fact that both sides of the sample need to be optically accessed. TIRFM is especially useful in imaging surface immobilized molecules or, in the case of (intra)cellular imaging, the basal plasma membrane and ~100 nm of the adjacent cytoplasm.

Highly Inclined and Laminated Optical Sheet (HILO) Illumination

Although TIRFM provides image quality greatly improved over that obtained by traditional epi-illumination, it is restricted to imaging molecules near an optically transparent surface. HILO microscopy (HILOM), also termed variable angle epi-fluorescence microscopy (VAEM) or near-TIRFM, overcomes this limitation by greater penetration into the sample without significantly compromising the signal-to-noise ratio (SNR) (21, 22). Similar to OTIRF, the light source is focused onto the BFP of the objective but at a smaller radial distance from the optical axis so that the incident angle does not exceed the critical angle. This way, light is refracted into the sample at high inclination from the optical axis, thus illuminating a small lamina within the sample, the width of which is dependent on the diameter of the field of view (FoV) and the angle of incidence. The laminar width of the beam is maintained by using a field stop, essentially decreasing the FoV, to prevent excessive divergence of the incident beam. Due to the transmission of the refracted beam through the objective into the sample, as in epi- and narrow-field illumination, any movement of the objective along the optical axis results in focusing on a different plane in the sample along the z-dimension, enabling imaging in 3D (21, 22). The excitation beam path for epi-illumination, OTIRFM and HILOM are relatively similar so that a single microscope can be used to implement all three schemes.

Narrow-Field Epi-Illumination

In narrow-field epi-illumination, light is focused onto a small volume element within the sample, thus exciting only molecules in the excitation volume and not those outside of it. Confocal laser scanning microscopes work by this principle, wherein focusing of light to a specific volume is achieved by introducing pinholes (or apertures) in the excitation and emission paths. Higher resolution as compared to wide-field illumination can be achieved by decreasing the width of the pinholes, but this comes at the cost of lower photon collection. The method also suffers from slow sample readout rates as scanning an entire specimen occurs at one volume element at a time. A significant improvement in the scanning rate can be achieved by using spinning-disc or Nipkow-disc confocal microscopy. A disc consisting of several microlenses spins at typically 3,500 rpm to create virtual pinholes for confocal detection (23), essentially exciting several distinct regions of the sample simultaneously.

LIGHT SOURCES AND DETECTORS

Lasers are preferred over lamps for high-resolution optical microscopy because of their monochromatic, coherent, and collimated light. Laser power should be high enough to excite all molecules optimally without damaging the sample. The wavelength of light spans anywhere from the far ultra-violet (UV) to the near-infra-red (NIR) region of the electro-magnetic spectrum (350–1000 nm), depending on the nature of the fluorescent probe and sample used. However, wavelengths from the visible part of the spectrum (450–680 nm) are used most frequently, mainly for two reasons. First, the transmission properties of available optics are best in the visible range, and second, most well-documented fluorescent probes (fluorophores) have their spectral properties in this region of the electromagnetic spectrum. Moreover, UV light is not suitable for imaging living cells: it induces DNA damage and sometimes even apoptosis (24). IR lasers are slowly gaining popularity, however, because they scatter the least, thus significantly improving sample penetration depth.

Charge coupled devices (CCDs) and avalanche photodiodes (APDs) or photomultiplier tubes (PMTs) are most commonly used in SMFM, and depending on the type of imaging performed, one or the other is preferred. In wide-field illumination, CCDs are the detectors of choice, whereas for narrow-field illumination where photons from only a small region of the entire sample are collected, APDs or PMTs are used. CCDs contain a large matrix of photosensitive elements (or pixels) that simultaneously collect photons over the entire detector surface. Photon flux information at each pixel is stored as an electronic charge (photoelectron) that is first converted to an analog voltage by an amplifier, then digitized. Intensified (I-)CCDs and electron-multiplying (EM-)CCDs amplify the number of photoelectrons through an external amplifier and on-chip, respectively, such that the digital number is (marginally) linearly dependent on the number of photons collected, making intensity values semi-quantitative at the (sub-)pixel level. APDs and PMTs are point detectors sensitive enough to detect and accurately count single photons, but have to be used in laser scanning microscopes to generate images of two-dimensional samples, limiting their time resolution. The time resolution obtainable with CCDs is primarily limited by the frame rate (number of frames or images per unit time), whereas the spatial resolution is dependent on the number of pixels and the quantum efficiency (i.e., the fraction of detected versus collected photons). A typical CCD used in SMFM has 512 × 512 pixels. While CCDs with higher numbers of pixels are available (e.g., 1024 × 1024), they are often less sensitive due to lower quantum yields.

PROBES

The sample or the single molecule(s) under inquiry must be conjugated to a (fluorescent) probe or carry strong inherent fluorescence to be visualized. Synthetic dyes (Cy dyes, Alexa dyes, various forms of rhodamine dyes), fluorescent beads, quantum dots, and fluorescent proteins (FPs) are among the common fluorescent probes used in SMFM. FPs are the mainstay of intracellular fluorescence microscopy. The cloning and expression of fluorescent proteins fused to cellular targets have become routine practices. However, this method of labeling comes at the cost that the protein fusion must be expressed exogenously, often resulting in overexpression, compared to endogenous

copies. Using inducible expression systems (25) is one of the many possible tricks that can be employed to mitigate overexpression. Non-fluorescent beads, especially ones of large size, can be imaged with high precision even using microscopes with simple optics, making them an attractive alternative to synthetic dyes and FPs in single particle tracking (SPT). Conjugating biomolecules to beads and to a certain extent FPs, however, comes with the caveat that the attachment of a bulky load could skew the molecule's function, localization, and/or diffusion. The development of various bio-orthogonal labeling strategies (26) and fluorogenic photo-affinity probes (27, 28) has made the specific labeling of single molecules with small fluorescent probes a viable option, even in living cells. A more detailed description and comparison of conjugation chemistries and the different organic dyes and FPs used in SMFM can be found in several reviews (29–31).

A fluorophore suitable for SMFM should have high brightness, favorable photophysical properties, and sufficient inertness so that the label does not interfere with the function of the molecule to be tagged. The first two criteria have a direct impact on the localization accuracy of single molecules. Brightness, a value of photon output that is calculated as the product of a fluorophore's extinction coefficient and quantum yield, should be high enough to delineate signal from noise. Undesirable photophysical processes, such as intersystem crossing (triplet state excitation) and photobleaching, markedly affect the quality and length of a single-molecule recording. Although the precise mechanism is unclear, molecular oxygen is thought to be primarily responsible for photobleaching via photo-oxidation of the fluorophore. Several chemical agents (e.g., cyclooctatetraene (COT), trolox, and 4-nitobenzyl alcohol (32)) and enzymatic oxygen scavenging systems (e.g., those containing glucoseoxidase and catalase (9) or protocatechiuc acid and protocatechuate-3,4-dioxygenase (33)) can be used to prevent fast photobleaching and quench triplet state excitation. Attaching multiple fluorophores per molecule can also increase brightness and fluorescence longevity, but it also increases the risk of rendering the molecule nonfunctional.

Imaging living biological samples presents a unique set of problems, including phototoxicity and autofluorescence. Fluorophores, in their excited states, react with molecular oxygen in the cell, resulting in the accumulation of phototoxic free radicals that can compromise subcellular compartments or even the entire cell's livelihood (34). Thus, a balance has to be struck between the excitation laser power (and wavelength) used and the time for which the sample is illuminated, especially for long time-lapse experiments. In addition, naturally fluorescent molecules present inside cells, such as NADH, FADH, and heme, absorb visible light and fluoresce, contributing to a high background level of autofluorescence during imaging. One way to circumvent autofluorescence and simultaneously enhance photostability of FPs is by using cell culture media that do not contain any fluorescent molecules, especially vitamins (35). Arguably the best solution is, however, to use fluorophore probes that absorb light in the far-red visible or NIR part of the spectrum where cellular components show minimal absorption (36, 37).

IMAGING SINGLE MOLECULES WITH NANOMETER SCALE LOCALIZATION ACCURACY

Even before the advent of single-molecule detection methods, there was a widespread interest in tracking the movement or diffusion of molecules, especially membrane

proteins and motor proteins, in solution and in living cells. Ensemble methods to calculate molecular velocities and diffusion coefficients have existed in the form of fluorescence correlation spectroscopy, or FCS (38), and fluorescence recovery after photobleaching, or FRAP (39). Tracking the movement of individual molecules with high spatio-temporal resolution seemed like a logical extension.

During the late 1980s, three different groups independently tracked the displacement of single beads over time by high-speed video microscopy both in vitro (40) and within living cells (41, 42) with ~10–100 nm lateral accuracy and sub-second temporal resolution. Around the same time, the optical absorption spectrum of single pentacene molecules was recorded in p-terphenyl crystalline matrices at liquid-helium temperature (43). Single-molecule fluorescence detection of cryo-cooled pentacene molecules soon followed (44, 45). In an effort to enhance resolution and extend single molecule detection to the third dimension, Van Oijen et al. (46) used a combination of confocal microscopy and spectrally selective imaging (SSI) to localize single pentacene molecules embedded in p-terphenyl crystals. SSI involves sequentially exciting individual pentacene molecules of distinct absorption maxima (caused by matrix effects), so that each molecule can be localized independent of the presence of another within a densely populated, otherwise un-resolvable region. The abilities to track beads with high accuracy and to visualize single fluorescent molecules with high resolution, together with a continual expansion of the available repertoire of optical instrumentation, have converged over the past two decades into what is now termed super-accuracy and super-resolution imaging.

A single fluorescent probe (or a cluster of closely positioned probes) can be considered to be a point source of emitted light whose image is, due to diffraction, spread over a much larger area on the detector than the actual size of the object. Such an image, referred to as a diffraction limited spot, appears as an airy disc, composed of a central bright spot surrounded by concentric rings of diminishing intensities. The intensity distribution of such an image can be mathematically described by what is termed a point spread function (PSF). By approximating the PSF with a simple two-dimensional (2D) Gaussian function, the intensity maximum, that is, the center of the Gaussian curve, can be localized with an accuracy similar in magnitude to the size of the fluorescent emitter, effectively breaking the diffraction barrier and Abbe's law.

FLUORESCENCE IMAGING WITH ONE NANOMETER ACCURACY (FIONA)

FIONA is a super-accuracy method that is used to localize and track single, typically fluorescently labeled, molecules with nanometer accuracy in the x-y plane (47). Fluorescence from single emitters is detected by a CCD and the intensity is plotted as a function of the spatial coordinates x and y (Figure 9.2a). The resulting PSF is fit with a 2D Gaussian function:

$$P_g(x,y;z_0,A,x_0,y_0,s_x,s_y) = z_0 + A\exp\left[-\frac{1}{2}\left[\left(\frac{(x-x_0)^2}{s_x}\right)+\left(\frac{(y-y_0)^2}{s_y}\right)\right]\right] \quad (3)$$

where z_0 is a constant term due to background fluorescence, A is the amplitude or maximal signal, x_0 and y_0 are the coordinates of the center of the distribution, and s_x and s_y are the standard deviations along the axes. The full width at half-maximum (FWHM) of the Gaussian depicts the variance of the PSF, and the (central) peak pinpoints the mean (Figure 9.2a). The variance divided by the number of photons collected results in the most simplistic form of the standard error of the mean (s.e.m.), or the precision by which the molecule can be localized (48, 49):

$$\left\langle (\Delta x)^2 \right\rangle = \frac{s^2}{N} \tag{4}$$

where Δx is the error in localization, $\langle(\Delta x)^2\rangle$ is the s.e.m., s^2 is the variance and N is the number of photons. The s.e.m. also depends on other important parameters, including the detector noise, background noise, and the effective pixel size (49):

$$\left\langle (\Delta x)^2 \right\rangle = \frac{s^2 + \left(\frac{a^2}{12}\right)}{N} + \frac{8\pi s^4 b^2}{a^2 N^2} \tag{5}$$

where a is the effective pixel size, which is simply the CCD pixel size divided by the overall magnification used, and b represents noise of any form. This equation shows that greater localization accuracy can be achieved by increasing the number of photons collected, decreasing the noise, and/or reducing the effective pixel size. High (1.2–1.65) NA objectives and back-thinned CCDs are typically used to collect as many photons as possible with minimal detector noise. Decreasing the effective pixel size requires a corresponding increase in magnification, which in turn reduces the number of photons collected per unit square area of the detector, significantly compromising the SNR. Therefore, a localization precision of 1–2 nm can be achieved under ideal conditions by collecting 5,000–10,000 photons using a CCD with effective pixel size of 80–120 nm. The same principles can be applied to each frame of a movie (or series of multiple frames), tracking the movement of a single molecule with ~1-nm accuracy, hence the name FIONA. Depending on the frame rate at which the movie is recorded, a temporal resolution of up to 1 ms can be achieved (47).

Perhaps one of the most convincing proof-of-concepts for FIONA, and a spearhead for the broader adoption of single molecule techniques, originated from the investigation of motor protein movements. The mechanism by which motor proteins translocate on a cytoskeletal "path" was under debate for several years. Myosin V is a dimeric-motor protein that contains a catalytic ("head") domain, a light chain "arm" that is composed of six calmodulins, and a cargo binding domain on each of its monomers that is held together by a coiled-coil "stalk" (Figure 9.2b). One study (50) postulated that kinesin, another motor protein, moves over microtubules by an "inchworm"-type mechanism, where one of the arms always leads, while another study (51) hypothesized a hand-over-hand mechanism, in which the two heads alternately move past one another. Yildiz et al. (47) resorted to FIONA to resolve the controversy. They used a myosin-light-chain-domain labeling strategy

similar to that used by Goldman and coworkers (51). Rhodamine-labeled calmodulin was added to myosin V monomers so that each dimeric motor protein contained a single fluorophore (i.e., one fluorophore per two arms). The labeled arm is expected to take alternative 37-2X nm and 37+2X nm steps if it translocates by a hand-over-hand mechanism, where X is the distance of the fluorophore from the stalk. For a labeled calmodulin closest to the head, X would be ~18.5 nm, and hence, the motor should take alternating 74 nm and 0 nm steps. Alternatively, if the motor moves by an inchworm type mechanism, the step size should be a constant ~37 nm. Not only could the authors convincingly show that the protein moved via a hand-over-hand mechanism by plotting the position of the fluorophore with time, they could also distinguish between molecules that had the labeled calmodulin at different positions with respect to the stalk (Figure 9.2c). Similarly, FIONA has also been used to track the path taken by kinesin as it "walks" over microtubules in vitro (52).

MULTI-LABEL IMAGING AND PARTICLE TRACKING

Single-Molecule High-Resolution Imaging with Photobleaching (SHRImP) and Nanometer Localized Multiple Single Molecules (NALMS)

In an effort to extend the use of FIONA to densely populated samples in which the PSFs overlap, both Paul Selvin's group (53) and Norbert Scherer's group (54) developed a method that exploits the quantized photobleaching behavior of single fluorophores to perform FIONA localization, and termed it SHRImP and NALMS, respectively.

The principle of SHRImP/NALMS can be explained by considering a sample that contains two molecules A and B whose PSFs overlap (PSF_A + PSF_B). If both fluorophores photobleach, the signal reduction in a plot of intensity over time will typically be in the form of two consecutive steps, each step representing the photobleaching of a single fluorophore, since it is highly unlikely for multiple fluorophores to photobleach at the same time. This stepwise photobleaching can be used to count the number of fluorophores with overlapping PSFs (55, 56). Once A has photobleached, the image only contains PSF_B, which can now be localized with high accuracy using FIONA. The resultant image can then be subtracted from the original image (PSF_A + PSF_B) to derive PSF_A, another single PSF to which the FIONA can be applied, thus localizing both molecules with high accuracy in different images of a movie. The same concept can be applied to a sample that contains more than two overlapping PSFs, enabling localization of molecules that are separated by as low as ~10 nm (53, 54).

Gordon et al. (53) used SHRImP to resolve double-stranded (ds) DNA molecules each labeled with one Cy3 at both 5′ ends. Upon imaging immobilized biotin-tagged DNA molecules of different lengths (30–50 bp) with TIRF, they deduced the expected length for each molecule of 3.4Å per base pair. Qu et al. (54) used NALMS to arrive at a similar conclusion, but in addition to using short dsDNA also used long λ-DNA hybridized to multiple Cy3-PNA conjugates to resolve up to ~20 serially overlapping PSFs, each separated by ~7 nm.

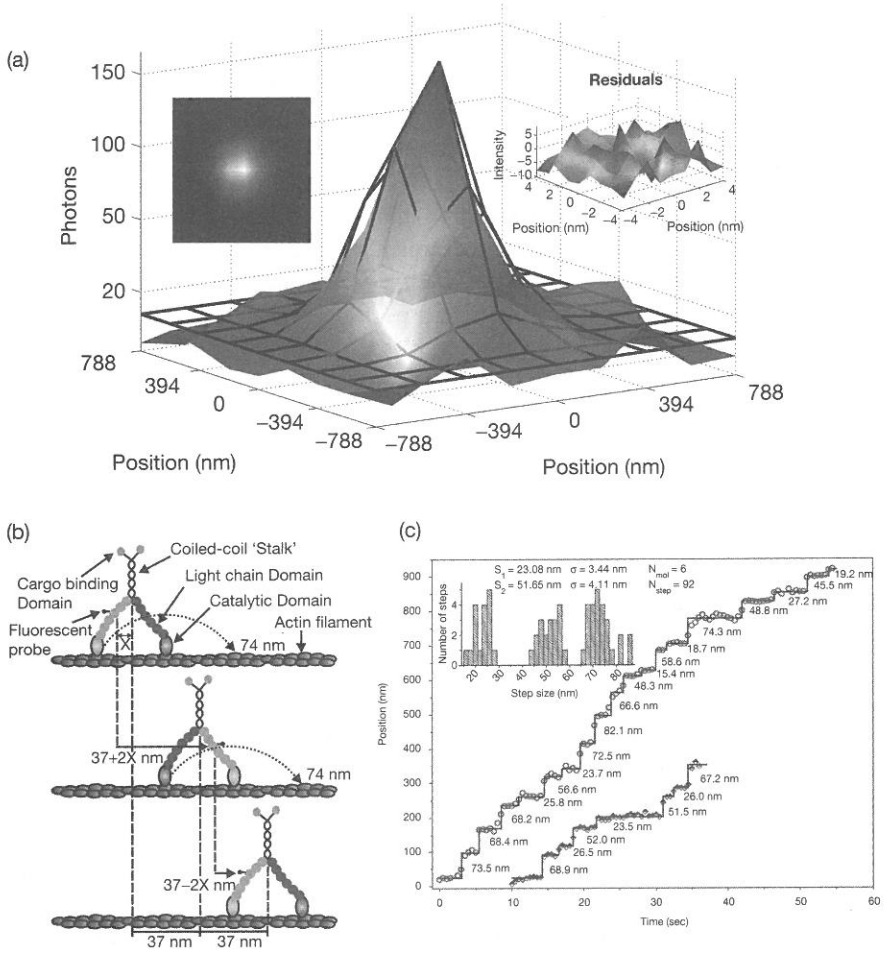

Figure 9.2 FIONA and its application. (a) CCD image of a single Cy5 labeled RNA (left inset) and its corresponding PSF fit to a 2D Gaussian. Residuals from the fit, which depict the deviation of data points from the fitted curve, are also shown (right inset). (b) The hand-over-hand translocation model of myosin V as evident from single molecule step traces of myosin V labeled with bifunctional rhodamine on one of the twelve calmodulin light chains (47). On average, the protein alternates between 52 nm and 23 nm steps as it moves. This stepping pattern suggests that X, the distance along the direction of motion between the center of the coiled-coil stalk and labeled calmodulin, is 7.5 nm, i.e., the third calmodulin from the top is labeled. Sometimes, the speed of myosin V translocation is much faster than the frame rate of image acquisition, due to which, some 52 nm and 23 nm steps combine to yield ~74 nm apparent steps. A histogram of six myosin V molecules taking a total of 92 steps, representing the frequency of occurrence of specific step-sizes, is shown in the inset. (Panel c reproduced with permission from (47)). See insert for color version.

Single-Molecule High-Resolution Colocalization (SHREC)

SHREC resolves overlapping PSFs originating from molecules labeled with spectrally distinct fluorescent dyes. Unlike SHRImP/NALMS, SHREC does not depend

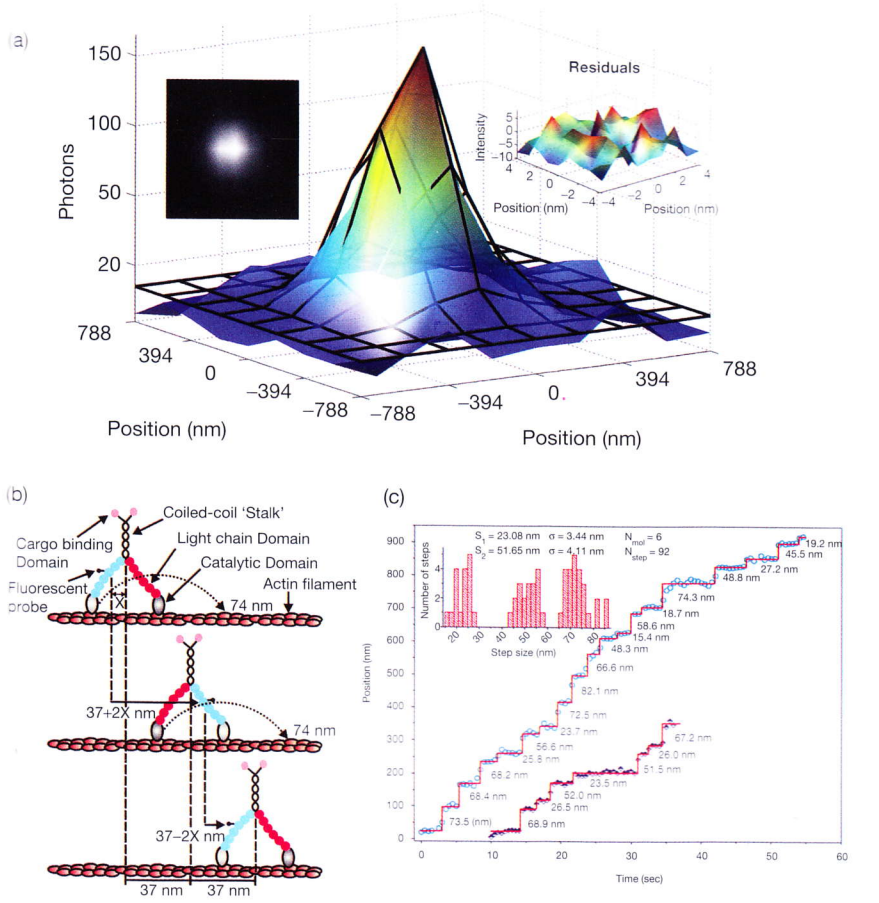

Figure 9.2 FIONA and its application. (a) CCD image of a single Cy5 labeled RNA (left inset) and its corresponding PSF fit to a 2D Gaussian. Residuals from the fit, which depict the deviation of data points from the fitted curve, are also shown (right inset). (b) The hand-over-hand translocation model of myosin V as evident from single molecule step traces of myosin V labeled with bifunctional rhodamine on one of the twelve calmodulin light chains (47). On average, the protein alternates between 52 nm and 23 nm steps as it moves. This stepping pattern suggests that X, the distance along the direction of motion between the center of the coiled-coil stalk and labeled calmodulin, is 7.5 nm, i.e., the third calmodulin from the top is labeled. Sometimes, the speed of myosin V translocation is much faster than the frame rate of image acquisition, due to which, some 52 nm and 23 nm steps combine to yield ~74 nm apparent steps. A histogram of six myosin V molecules taking a total of 92 steps, representing the frequency of occurrence of specific step-sizes, is shown in the inset. (Panel c reproduced with permission from (47)).

on photobleaching of fluorescent probes so that the observation window for imaging can be significantly extended (57). However, it requires the precise mapping of images from channels of distinct spectral range (color) onto one another, which is nontrivial due to chromatic aberrations of the optics. Spudich and coworkers therefore developed a mapping calibration for SHREC that uses fiduciary markers to measure the registration between the color detection channels. To this end, surface immobilized beads of sub-diffraction (100 nm) diameter labeled with both Cy3 and Cy5 (fiduciary markers) were imaged at such a low density that only a single bead was visible per FoV. This bead was then moved in 0.5-μm steps in the pattern of a 12×26 grid with a piezoelectric stage. The resultant 312 images were stacked to create a single image containing 614 regularly spaced PSFs (312 each in the Cy3 and Cy5 channels). Each PSFs in each channel was independently fit with a 2D Gaussian function and localized by a FIONA-like algorithm. Combining all locations thus determined, a local weighted mean transformation (58) was calculated to map any point in the Cy5 channel precisely onto its corresponding point in the Cy3 channel. The resultant map is used as a template to localize single dual-labeled molecules.

To benchmark their SHREC technique, the authors used Cy3/Cy5 doubly labeled dsDNA similar to that used in the SHRImP and NALMS studies and obtained very similar results (57). They then went on to use SHREC to concomitantly visualize the movement of both legs of myosin V in real-time. To this end, they exchanged the native calmodulines with a mixture of either Cy3- or Cy5 labeled calmodulins so that, on occasion, the two legs of a myosin would carry each a different fluorophore. As expected, they observed leg step sizes of ~74 nm, shifted by ~37 nm between the two color channels (57). More recently, Singer and coworkers have used a similar super-registration approach to track the transport of β-actin mRNAs through the nuclear pore complex (NPC). By achieving an unprecedented ~20-nm lateral accuracy at ~20-ms time resolution in living cells, they observed and measured the kinetics of a fast three-step mRNA transport process taking no more than 200-ms total time (59).

Of note, the multi-fluorophore super-accuracy imaging methods SHRImP, NALMS, and SHREC are closely related to and likely inspired the super-resolution imaging techniques, such as STORM and PALM discussed below. The primary goal of the former methods is to localize and track single or few molecules over time with high precision, whereas the latter tools aim to resolve ~10^3 times higher densities of single molecules over consecutive imaging cycles where only few molecules are turned on at any given time, accumulating data for a super-resolution image over time.

LOCALIZATION AND TRACKING OF SINGLE MOLECULES IN 3D

Initial efforts in SPT involved systems that were either two-dimensional in nature, such as labeled lipid molecules in the basal membrane of a cell, or the information obtained were 2D projections of objects moving in 3D. Verkman and coworkers developed a unique method for 3D SPT by introducing a cylindrical lens in the optical path of an epi-fluorescence microscope (60). The PSF of a particle in focus then is circular in shape and becomes larger and more ellipsoidal when the particle moves out of the focal plane. The major axis of the ellipsoid formed when the particle is above the focal plane is perpendicular to that formed when the particle is below

the focal plane. Using this method, the authors localized red fluorescent beads of 100-nm diameter in living cultured cells with ~5-nm lateral and ~12-nm axial accuracy at ~500-ms time resolution (60).

Another powerful method for tracking particles in 3D is off-focus or defocused imaging. Developed by Florin and coworkers this method is based on the principle that the diameter and pattern of a PSF varies as the object is defocused (61). Particles that are slightly out-of-focus have a larger PSF diameter than when in focus and those even further from the focal plane give rise to a complex ring patterned PSF. The distance of the particle from the image plane can be deduced from the intensity pattern of the rings (i.e., the number, diameter, and relative intensity of rings). Schutz et al. used this method to record the trajectory of single potassium channels labeled with Cy5-tagged hongotoxin ligands in living T-lymphocyte cells (62). Although the method yielded lower axial accuracy than bead tracking (~40 nm versus ~3 nm), it was the first report of 3D SPT of molecules tagged with small fluorescent probes. Toprak et al. (63) used a variation of the above method to track phagocytosed beads with ~2.7-nm lateral accuracy and ~3.7-nm accuracy along the optical axis at 50-ms time resolution. In this technique, termed bifocal imaging, only 30 percent of the emitted light is focused, leaving the other 70 percent defocused, both of which are then split onto different regions of a CCD camera. The focused and defocused PSFs of a single particle are first mapped onto one another and then used to record the trajectory of the particle in the x-y plane and the z-axis, respectively.

Another approach for 3D SPT is based on the relative displacement of a pair of split images of the PSF onto distinct regions of the CCD. Appropriately named *Parallax* by Goldman and coworkers, either a wedge prism (64) or two closely spaced, parallel mirrors (65) are introduced at the back-focal-plane of the objective to view a fluorescent particle from two sides of the optical axis of the objective. With this optical configuration, the image of a particle moving in only the x-y plane is equally displaced in the x and y directions on either region of the CCD. By contrast, movements along the z-direction are reflected by the two images moving towards or away from each other in the x- (64) or y-direction (65). The authors localized fluorescent particles with ~3-nm accuracy along the optical axis, including glucose-transporter containing vesicles in living adipocytes and single myosins walking along actin filaments (65, 66).

Finally, Moerner and coworkers recently introduced a so-called 4*f* imaging system composed of two achromatic lenses and a reflective liquid crystal phase-only spatial light modulator that convolves the microscope image with a double-helical PSF (67, 68). As a result, the camera image obtained of a single fluorescent particle shows two spots whose relative x,y-positions will twist around each other as the z-position of the tracked particle changes (like the two backbones of a dsDNA viewed along the double-helical axis). The authors were able to localize brightly fluorescent 200-nm beads with ~5–10-nm precision in the z-dimension and weaker emitters with up to ~30-nm precision (68).

SUPER-RESOLUTION IMAGING BASED ON SINGLE-MOLECULE LOCALIZATION

The emergence of single-molecule techniques, such as FIONA, demonstrated the ability to break the classical optical diffraction barrier and provide super-accuracy

resolution in determining a single fluorescent molecule's localization. Since a conventional wide-field image of a cell containing many fluorescent molecules can be thought of as a distribution of diffraction limited spots, it should then be possible to extend FIONA from a single-molecule "super-accuracy" approach to a method for obtaining the bigger picture: complete "super-resolution" images of macromolecular structures and assemblies.

The main challenge in applying FIONA to super-resolution imaging of cells is that FIONA requires well-isolated point sources. As the signals from multiple points begin to overlap, the diffraction pattern becomes distorted and the model for fitting the PSF begins to break down, causing decreased localization accuracy. For this reason, FIONA has mostly been applied to single molecule studies where the concentration of the molecule of interest can be kept low. If the goal, however, is to image a subcellular structure, then that particular structure must be labeled with a minimum number of point sources to construct an image with enough information to define its shape and contours. To prevent under-sampling and ensure accurate and complete imaging, the Nyquist-Shannon theorem postulates that the sampling interval must be at least half that of the desired resolution (69). Thus, to obtain an image with 50-nm lateral resolution, the labeling point sources must not be more than 25 nm apart in the x,y-plane. This translates into a high labeling density of at least $6.4 \times 10^3/\mu m^2$ or ≥ 200 points per diffraction-limited area (when imaging a fluorophore with emission wavelength $\lambda = 550$ nm with an objective lens of NA = 1.45).

In the first half of the 2000s, several groups worked to extend FIONA to samples with more than one label, which led to the development of SHREC and SHRImP/NALMS described above. These techniques resolve two dyes separated by < 10 nm—a considerable improvement, yet still not able to handle the densities required for subcellular super-resolution imaging. Around the same time, photoswitchable proteins and dyes were undergoing rapid development. In response to certain wavelengths of light, these fluorescent proteins undergo conformational changes that alter their fluorescence properties—turning them "on" or "off," or causing a shift in the spectral profile. The first photoswitchable protein discovered, Kaede, was cloned from the coral *Trachyphyllia geoffroyi* and irreversibly converts from a green to a red fluorescent protein upon irradiation with UV or blue light (70). Several other fluorescent proteins have since been engineered using high-throughput mutagenesis to have similar photoreactive properties. In addition, a photoswitchable small molecule dye formed between the cyanine dyes Cy3 and Cy5 was reported (71). These new fluorescent markers were immediately recognized for their potential in cell, organelle, and protein tracking experiments using existing imaging strategies (72). However, it took four years after the discovery of Kaede to realize the full potential of photoswitchable probes in super-resolution imaging.

STORM/PALM/F-PALM

In 2006 three groups independently published methods that take advantage of photoswitchable probes for super-resolution imaging based on single molecule localization (SRI-SML) termed, respectively, stochastic optical reconstruction microscopy (STORM) (73), photoactivation light microscopy (PALM) (74), and fluorescent photoactivation light microscopy (F-PALM) (75). Although different in name, these

methods all rely on the same basic principle: By sparsely activating or "turning on" only a small subset of the total number of photoswitchable probes in any given video frame, the *effective* labeling density for that frame becomes sufficiently low to allow each activated probe to be localized with FIONA. Applying this concept, image acquisition proceeds in an iterative manner where the series of events—activation, readout, inactivation—is continuously repeated until enough molecules are localized to fulfill the Nyquist criterion for the desired resolution (Figure 9.3a). The final image is then reconstructed or mapped by super-positioning the coordinates of the probes localized for each frame onto the same reconstructed image. A Gaussian peak represents each particle whose width represents the uncertainty in localization. Therefore, the resolution of the final image is determined by only two factors: the localization accuracy from FIONA and the density of localized probes.

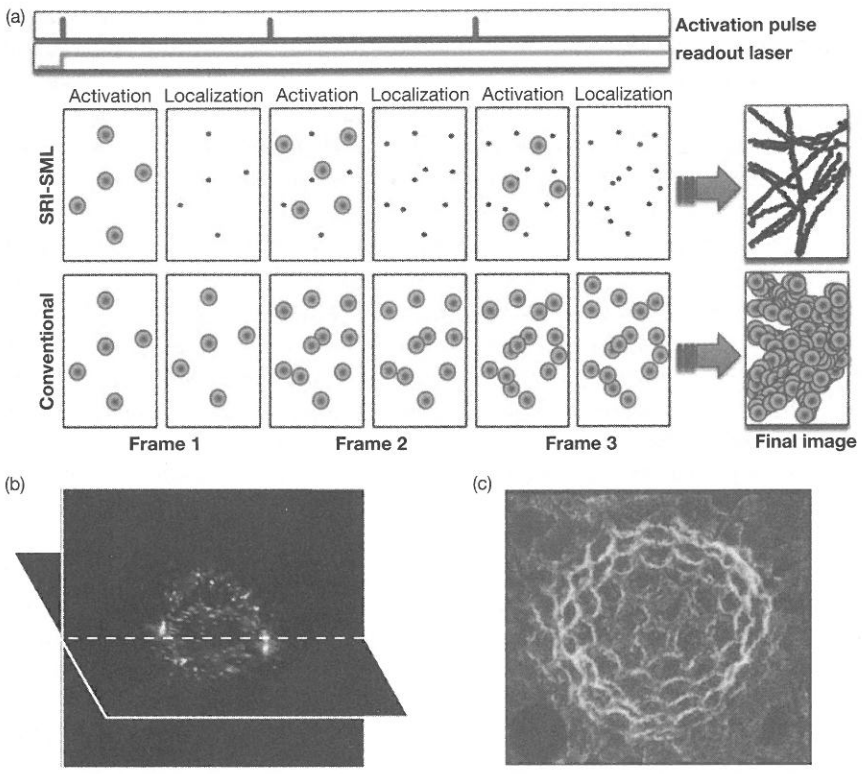

Figure 9.3 Comparison of SRI-SML imaging with conventional fluorescence and electron microscopy. (a) SRI-SML images have a much higher resolution compared to conventional fluorescence microscope images. This resolution enhancement is particularly striking in the case of microtubule filaments. As illustrated, due to overlapping of diffraction-limited spots, conventional imaging cannot resolve single filaments or capture the intricate criss-crossing pattern clearly observed in SRI-SML images. Note that, unlike SRI-SML, conventional imaging only requires one frame per image, thus the final image is not built up upon individual activation events. Individual frames are illustrated here merely for the sake of comparison. (b) and (c) Comparison of images of clathrin coated pits obtained using 3D STORM and electron microscopy (Reproduced with permission from (98, 133)). See insert for color version.

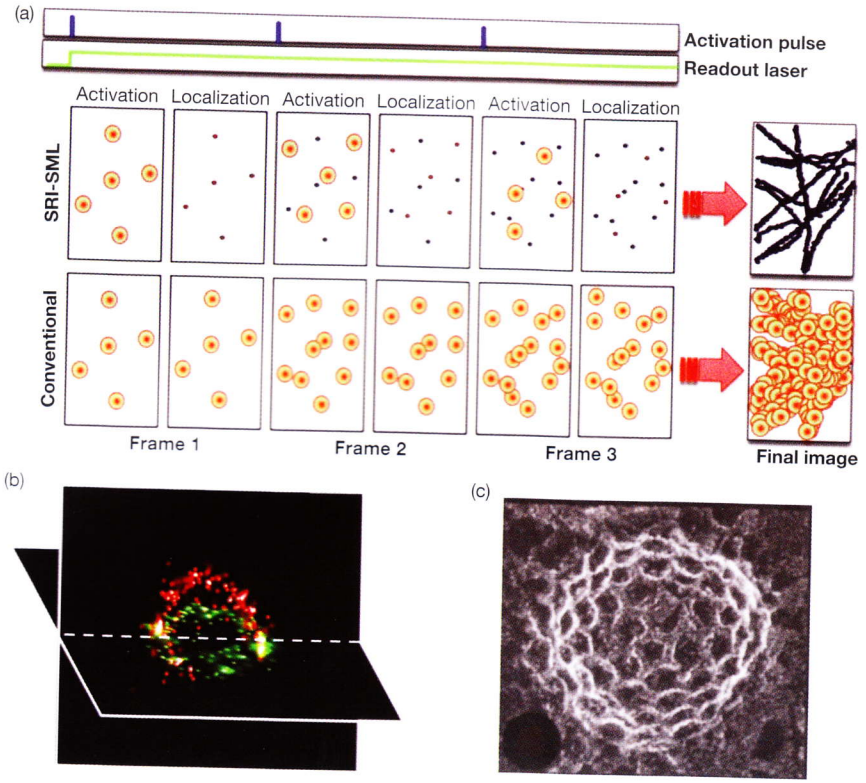

Figure 9.3 Comparison of SRI-SML imaging with conventional fluorescence and electron microscopy. (a) SRI-SML images have a much higher resolution compared to conventional fluorescence microscope images. This resolution enhancement is particularly striking in the case of microtubule filaments. As illustrated, due to overlapping of diffraction-limited spots, conventional imaging cannot resolve single filaments or capture the intricate criss-crossing pattern clearly observed in SRI-SML images. Note that, unlike SRI-SML, conventional imaging only requires one frame per image, thus the final image is not built up upon individual activation events. Individual frames are illustrated here merely for the sake of comparison. (b) and (c) Comparison of images of clathrin coated pits obtained using 3D STORM and electron microscopy (Reproduced with permission from (98, 133)).

Unlike "hardware-based" super-resolution techniques (see final section below), SRI-SML does not require custom microscope components, lending itself to retrofitting of existing equipment. The basic setup consists of an inverted epi-fluorescence microscope equipped with a high NA objective lens, scientific grade EM-CCD camera, and a pair of continuous wave lasers. Often an objective-type total internal reflection (TIRF) or near-TIRF/HiLo illumination configuration is used to reduce background. Two lasers are typically used to drive the acquisition cycle—a weak short-wavelength laser for activation and a higher power longer-wavelength laser for readout and inactivation. The lasers are either sequentially alternated with a longer duration for readout/inactivation, or the activation laser is pulsed at appropriate intervals while the longer-wavelength laser continuously illuminates the sample. Each fluorophore exhibits unique switching kinetics, but in general, laser induced switching rates are faster than spontaneous rates and are linearly dependent on laser intensity (71). The activation laser intensity is optimized to activate the maximum number of molecules per frame without overlap, usually ~1 per μm^2 area (76). Since acquisition rates are largely limited by the off-rate of switching, the laser used for readout and inactivation is often set to a high intensity. The frame rate of the EM-CCD camera is often synchronized with the switching events, wherein the exposure times for each frame match the average fluorescence on-time of activated probes. Typical frame rates are on the timescale of 30–100 ms (a first-order approximation for the frame rates required for a particular fluorophore can be found in reference (76)). To simplify the acquisition process, asynchronous camera schemes (i.e., protocols that do not match the camera acquisition time to the duration of photon bursts) have also been demonstrated (77, 78).

The first studies with STORM/PALM/F-PALM produced striking images at a resolution nearly an order of magnitude greater than the diffraction limit. Zhuang and coworkers imaged individual RecA DNA binding proteins bound to plasmid DNA with ~ 40-nm x,y-resolution by indirect immunofluorescence wherein the secondary antibody was labeled with a reversibly switchable synthetic dye (73). Hess and colleagues achieved similar resolution when imaging lysosomal transmembrane protein CD63 fused with Kaede in Cos-7 cell cryosections (74). With this improved resolution, it was possible to distinguish closely spaced lysosomal particles that may have been interacting or undergoing transformation from late endosomes. In comparison, standard wide-field fluorescence images of the same sample showed these closely spaced endosomes as a single uniform object. The extraordinary imaging power of these techniques was further demonstrated with several other targets, including the cytochrome-C oxidase import sequence localized within the mitochondrial matrix, vinculin and actin proteins located at focal adhesion regions of fox lung fibroblast cells, and the HIV1 Gag protein within intact Cos-7 cells (74).

Since photoswitching mediated SRI-SML is a single-molecule technique, it can be used to derive quantitative data on the spatial distribution of dense molecular assemblies. Single molecule localizations enabled Owen et al. (79) to compile 2D clustering maps of proteins in the cell membrane. Using a statistical analysis of adjacent particles, the authors found that a truncated form of the tyrosine kinase Lck, fused to the photoactivatable protein tdEos, heterogeneously distributes throughout the membrane with 58 percent of molecules localizing in clusters of various sizes, ranging between 20–190 nm in radius. Another membrane bound tyrosine kinase, Src, has a different distribution pattern when expressed in the same cells. Similar

protein counting experiments have been demonstrated using immunofluorescence staining of mitochondrial proteins (79). In addition to positional information, data on the orientations of molecules can also be derived. Gould et al. (80) determined the anisotropies of single actin and hemagglutinin proteins in fixed fibroblast cells by introducing a polarizing beam splitter in the detection path. Refinement of this approach could one day allow detection of the binding states of large populations of single molecules in cells. The marriage of SRI-SML with other single-molecule techniques, such as fluorescence resonance energy transfer (FRET), represents the current vanguard of technical development.

Switchable Probes for SRI-SML

The ideal probes for SRI-SML have photophysical attributes that maximize SNR. First and most importantly, probes should have a high photon output in the activated fluorescence on-state. Ideally, this output should occur rapidly and the on-state should be short-lived to decrease the necessary acquisition time. Second, the on-state should be several thousand-fold brighter than the off-state. Probes with a high contrast ratio between states will have the least amount of background. Third, the spontaneous interconversion rates between states should be much slower than the laser-controlled conversion rates to ensure that the number of activated probes in a given frame can be kept sufficiently low in a user-controlled manner.

A number of photoactivatable probes are currently available and fall within two categories: synthetic dyes and genetically encoded fusion proteins. Under current convention, the distinguishing factor between STORM- and PALM-type techniques is the category of probe used; STORM utilizes synthetic dyes while PALM utilizes fusion proteins. Both types of probes have several strengths and weaknesses, and neither is considered to be perfect. The best type of probe for any given experiment must be chosen on a case-by-case basis, depending on the molecular target, cell type, and overall goals of the experiment. Here, we juxtapose these two categories of photoactivatable probes in the context of SRI-SML and briefly highlight a few of the most commonly used probes under each category.

Synthetic Dyes

The most common synthetic switches are composed of cyanine dyes, a popular family of fluorescent dyes noted for their brightness due to large extinction coefficients. The original switchable synthetic dye used in STORM was composed of an activator Cy3 molecule and reporter Cy5 molecule (73). With this switch-pair, Cy5 emission is induced with red laser light and subsequently inactivated spontaneously by the same laser. Activation is induced using green laser light, which excites Cy3 and causes an energy transfer loosely analogous to FRET, which activates Cy5 but does not directly induce Cy5 emission in the absence of red laser light. Switching is reversible and can occur up to 1000 times before permanent photobleaching, enabling multiple localizations for each probe.

The exact mechanism of photoswitching is ill understood. High-resolution mass spectrometry suggests that Cy5 is switched into a reversible dark state by formation of a thiol-dye adduct produced by primary thiols, a required buffer component for switching, covalently bonding to the polymethine bridge of Cy5 (80). The role of

Cy3 in activation is less clear, and in fact, switching has been demonstrated in the absence of an activator dye, albeit at a much slower rate (30, 81). Cy3 can also be replaced by other fluorophores to serve as activators. Since the highest activation rates are induced with light at a wavelength corresponding to the maximum absorption wavelength of the activator, these alternative switch-pairs are convenient tools in multi-label SRI-SML (see below).

Typically, synthetic dyes must be conjugated to antibodies that bind to specific cellular proteins. Initially, antibodies for immunofluorescence were labeled with Cy3-Cy5 pairs by reacting amine-modified antibodies with dye mixtures containing amine-reactive Cy5 and an excess of Cy3 to increase the likelihood of each Cy5 label being closely adjacent to at least one activating Cy3 molecule (73). This process was later streamlined by directly conjugating Cy3 and Cy5 together, using commercially available starting materials (82). At ultra-high resolutions, one must consider the size of the fluorescent probe; greater distances between the probe and the target will reduce resolution. Despite the fact that synthetic dyes are >30-fold lower molecular weight than fluorescent proteins, the need to use randomly labeled antibodies as an intermediary considerably increases the "effective" size of the label. The effect of label size is significantly pronounced with microtubules, where antibody staining in STORM increases the apparent diameter of the cytoskeletal polymers to nearly double that of their true width of ~25 nm (83). The use of Fab fragments or direct immunofluorescence improves resolution. Additionally, biarsenical fluorophores derived from fluorescein, resorfin, and Cy3 have been developed that can bind specifically to short genetically encodable tetracysteine tags (84–86). Although switching with these fluorophores has not yet been reported, the potential exists for development of switchable analogues. Caged rhodamine derivatives featuring fluorescence-dampening protective groups, which are released in response to UV light, have recently been used in SRI-SML (74, 87). This chemistry can be applied to several other types of fluorophores, including biarsenicals, thus opening the door for the future direct labeling of cellular proteins with small, switchable, synthetic dyes.

Fluorescent Fusion Proteins

Switchable fluorescent proteins can be categorized into photoactivatable proteins that can be reversibly or irreversibly switched between a non-fluorescent off-state and a fluorescent on-state, and photoconvertible proteins whose emission changes color after activation with UV (405 nm) or blue (488 nm) light.

Two of the most popular switchable proteins are Dronpa and EosFP. Dronpa, engineered from the coral *Pectiniidae*, is a monomeric photoactivatable protein with a dark inactivated state and a green (518 nm) emission after activation with UV light. It is the one of the few reversibly switchable proteins and undergoes ~100 switching cycles. The switching mechanism is understood to involve a cis-trans isomerization of the chromophore that triggers further rearrangements of four proximal amino acids (88).

Dronpa has the highest extinction coefficient and contrast ratio of all switchable proteins, yet suffers from problematic switching behavior that ultimately affects its performance. In fact, PS-CFP2, a photoconvertible protein with a nearly two-fold lower extinction coefficient and higher background, could be localized more precisely than Dronpa in live cells (89). Several other variants have been engineered from Dronpa to improve or alter its switching properties (90, 91). EosFP,

a photoconvertible protein isolated from the coral *Lobophyllia hemprichii*, exists as a tetramer in its native environment, but monomeric forms have been engineered (92). In response to UV irradiation, a peptide bond near the chromophore undergoes a cleavage reaction, causing the green (569 nm) emission to be bathochromatically shifted to orange (581 nm) (93). EosFP is currently the brightest switchable fluorescent protein, leading to an excellent contrast ratio, and is largely considered the best switchable fluorescent protein available for SRI.

Multi-Label Imaging

A powerful feature of fluorescence microscopy is the ability to visualize multiple targets in a single sample, wherein each target is labeled with a spectrally distinct probe. A broad color palette of fluorescent probes has now made conventional fluorescence imaging with up to four colors commonplace. When combined with objective lenses corrected for chromatic aberration, these images become unparalleled analytical tools for monitoring the relative spatial distributions of cellular macromolecules. Analysis of such images can vary from qualitative evaluations to quantitative measurements; either way most often the fundamental derived facet indicative of molecular interaction is spatial colocalization. Several methods for defining colocalization exist; yet regardless of the analytical method applied, the biological significance of colocalization ultimately depends on image resolution. Targets that appear to be colocalized or interacting may, in fact, be merely proximal to one another at an unresolvable distance. Multi-label SRI-SML thus has the potential to improve our current knowledge of molecular interactions and distributions in cells.

The combinatorial pairing of cyanine activator and reporter dyes has created a pallet of distinct synthetic switch-pairs for STORM imaging. Switches consisting of Cy3 activators and far-red reporter dyes, such as Cy5, Cy5.5, and Cy7, can all be activated and read out with green and red (657 nm) laser light, respectively, and their signals can be unmixed with dichroic mirrors and bandpass emission filters. Alternatively, spectrally distinct activators—Alexa405, Cy3, and Cy2—have been paired with a Cy5 reporter and selectively activated with minimal cross-talk using laser light corresponding to the absorbance of each activator dye. An advantage of this strategy is that fewer laser wavelengths are needed compared to multiple color readout. By alternatively activating Cy2-Alexa647 (the latter a structural analog of Cy5) and Cy3-Alexa647, Bates et al. (93) were able to reconstruct two-color images of microtubules and clathrin-coated pits in fixed mammalian cells. Huang et al. (94) imaged Alexa405-Cy5 labeled mitochondria and A555-Cy5 labeled microtubules and observed an inchworm-like interaction where only portions of the mitochondria were in direct contact with the microtubules. Conventional TIRF images obscured these details and instead the microtubules appeared to be in direct contact along the full length of the mitochondria.

Multi-label imaging with fluorescent proteins is currently more challenging. The complication is that, unlike the multiple pairings of synthetic dyes, photoactivatable fluorescent proteins largely lack diversity. That is, they are similarly activated with UV-light, and their activation transitions fall into either one of two categories: from dark (non-fluorescent) to green emission or from green to orange emission. Since the signal from the preactivated form of the latter overlaps with the activated form of

the former, this precludes the possibility of simply using complementary probes from each category. Even though dark-to-red photoactivatable fluorescent proteins have been discovered, they are generally plagued by poor contrast ratio, although recent derivatives of mCherry are sufficient for use in live-cell PALM (94, 95). One strategy for overcoming this lack of spectral diversity is to take advantage of another unique attribute: reversible switching. Dronpa and EosFP can be concurrently activated yet imaged serially by first collecting the orange emission of EosFP and then, after irreversible inactivation or bleaching of all EosFP molecules, collecting the green emission of Dronpa without interference from EosFP's preactivated state (89). While a clever workaround, this technique is not suitable for live cell imaging since the target proteins will diffuse over time. Future development of unique fluorescent proteins will lead to new possibilities for multi-label imaging. As an example, Andresen et al. (97) engineered a new variant of Dronpa aptly named Padron (a reordering of the letters in Dronpa) that undergoes inverse or "positive switching" in which blue light activates and excites the green fluorescent protein and UV-light switches the protein off. Although Padron has not yet been used for SRI-SML, multi-label imaging with Padron and another Dronpa variant, rsFastlime (whose switching characteristics are similar to Dronpa), was demonstrated in living budding yeast cells by 3D confocal microscopy (96).

3D Imaging

At their inception, STORM and PALM were applied to a single focal plane of a sample and the improvement in lateral resolution was not extended to the z-dimension. To enable complete 3D reconstructive mapping of cells, several modified versions have been devised, many of which were inspired by the pioneering efforts in 3D SPT (discussed above). In 2008 Zhuang and colleagues published two methods for 3D STORM utilizing either a cylindrical lens or focal plane scanning (97, 98). Both methods produced similar results with resolutions as high as 20–30 nm lateral and 50–70 nm axial. By combining these methods with multi-label imaging, it was possible to visualize complex mitochondrial networks entangled within a 3D matrix of crisscrossing microtubules and the spherical cage-like shape of clathrin-coated pits containing structural details approaching those of electron microscopy (Figures 9.3b and 3c). However, one disadvantage of these techniques is their limited use in imaging thick samples. Cylindrical lens-based methods can only accurately localize molecules within < 600 nm of the focal plane and must be coupled with focal plane scanning to increase image depth. While biplane detection can achieve similar resolution with a slightly enhanced axial localization range independent of focal plane scanning, and with increased image depth (up to 4 μm) when coupled with scanning (99), there still exists an intrinsic limit in imaging depth caused by scattering of the emission light as it passes through a thick sample.

Multi-photon microscopy overcomes this obstacle by using short pulses of longer wavelength light to excite the fluorophore. Pioneered by Webb, two-photon excitation (TPE) overcomes many of the problems pertaining to conventional fluorescence microscopy—limited penetration depth of incident light, loss by scattering of emitted light, and background due to cellular autofluorescence. TPE is based on the principle that two photons can also excite a fluorophore in one quantum event

when the sum of energies of both photons equals that of the absorption energy of the fluorescent probe. The same principle can also be extended to multiple photons in which case the scheme is referred to as multi-photon excitation (MPE). As excitation by two photons is less probable than excitation by a single photon, higher light intensity is required for excitation (more than twice that required for single-photon excitation). TPE has mostly been used for imaging tissues or even live animals (100) but has recently gained popularity in high-resolution intracellular SMFM and SPT (101, 102). By combining two-photon microscopy with temporal focusing, which reduces background by minimizing the excitation volume, Vaziri et al. achieved PALM images over an axial depth of ~10 μm in mammalian and *Drosophila* S2 cells (103).

Live-Cell Imaging

To gain a better understanding of the molecular dynamics involved in biological processes, the ultimate frontier of super-resolution imaging has become the living cell. Live-cell SRI-SML is currently limited to imaging relatively slow dynamic events in a select set of cell lines. Since STORM/PALM/F-PALM requires many frames to build a single image, data acquisition rates are slower than conventional wide-field fluorescence microscopy. This ultimately precludes SRI-SML from imaging biological processes that unfold at rates faster than the acquisition rate limit. The prolonged exposure time and high laser power also requires samples that are tolerant to photo-induced damage. Several mammalian cell lines, including Chinese hamster ovary (CHO), NIH 3T3 fibroblasts, and African green monkey kidney Cos-7 cells, remain healthy under the harsh imaging conditions and resistant to changes in morphology after exposure (82, 104). Using these photo-tolerant cells and PALM, Shroff et al. (103) visualized the movements and dynamic organization of adhesion complexes (ACs)—networks of nearly 100 proteins involved in cellular motility and anchoring, organized in a thin lamina at the cell-(extra-cellular) matrix interface. By capturing frames every 40 ms and grouping 750 frames into single images, the formation, elongation, and retraction of ACs were imaged with a lateral resolution of ~70 nm and a temporal resolution of ~30 s. Since ACs evolve slowly at a rate of 120 nm/min, the movement of ACs over the course of a single frame was small enough to prevent blurring. In addition to imaging in living eukaryotic cells, SRI-SML has also been applied to *Caulobacter crescentus* bacteria (82, 105, 106).

The photoswitching-based imaging methodology of SRI-SML can also be combined with SPT to investigate faster dynamic processes. In this way, the goal is not to build a super-resolution image, but rather to measure the displacement of particles over short time and length scales as discussed earlier in the chapter. The incorporation of photoswitching-based imaging enables tracking of a small subset of molecules at a given time duration within densely populated structures, such as cell membrane domains or lamellipodia, which would be difficult or almost impossible using conventional SPT (107–109). In this case, cellular over-expression of the target is of advantage as it allows one to collect many more tracks from a single cell, increasing the statistical power of the analysis while decreasing imaging time.

SUPER-RESOLUTION MICROSCOPY—HARDWARE (OPTICS)-BASED METHODS

Beginning with confocal microscopy, several imaging techniques were developed starting in the 1990s with the vision of increasing resolution by reducing the focal spot size. These methods use specialized optical setups and can be considered "hardware-based" solutions for super-resolution imaging, as opposed to "software-based" methods like STORM/PALM/F-PALM, which rely instead on mathematical processing of a series of acquired diffraction limited images. Spot-scanning 4Pi microscopy (4PiM) (110) and wide-field I^5M (111) are two hardware-based techniques that can achieve ~3–7-fold greater axial resolution than traditional confocal microscopy. 4PiM uses two opposing high-NA objective lenses to illuminate a single focal spot. The coherent addition of wavefronts from both lenses narrows the focal dimension across the optical axis, resulting in higher resolution. I^5M implements the same opposing lens aperture enhancement for the detection of fluorescence but uses plane-parallel standing waves to illuminate the entire FoV.

Reversible Saturable Optical Fluorescence Transitions (RESOLFT) Techniques

RESOLFT techniques utilize sophisticated excitation configurations to physically decrease the width of the excitation volume and thus decrease the size of the PSF below theoretical limits of diffraction (112). These techniques can be described as targeted illumination/readout methods that do not require detection of single molecules, whereas STORM/PALM/F-PALM are stochastic readout methods based on the very features of single molecule detection. Implementation of RESOLFT can be loosely divided into three categories—stimulated emission depletion (STED) (113), ground state depletion (GSD) (114, 115), and saturated pattern excitation microscopy (SPEM)/saturated structured illumination microscopy (SSIM) (116, 117). In STED, two laser beams are used (Figure 9.4a), an excitation beam and a comparatively red-shifted "depletion" beam. The excitation laser is first applied, followed immediately (within picoseconds) by a doughnut-shaped depletion beam that depletes the excited state of all fluorophores except those at the very center of the original excitation beam. Fluorescence from the remaining molecules in the center of the focal volume is then detected. The intensity of the depletion beam can be increased to "squeeze" the final detection volume to a smaller size. The two beams are raster-scanned across the entire sample to form the complete image, as is generally done in scanning laser confocal fluorescence microscopy (16). Using STED microscopy, GFP-labeled viruses and endoplasmatic reticulum were imaged in fixed PtK2 cells with a lateral resolution of ~70 nm (118). Recently, Hell and coworkers implemented STED in a 4Pi microscope to achieve 40–45 nm in all three spatial dimensions by generating a spherical focal spot of the same diameter (119). Axial scanning of fixed Vero cells with this configuration revealed that immunologically labeled Tom20 (a subunit of the TOM complex) formed distinct clusters on the mitochondrial membrane. The group also implemented a dual-color imaging scheme in which they used a combination of two excitation-one depletion events to image both Tom20 and mtHsp70 (a mitochondrial matrix protein) simultaneously with ~40-nm resolution in 3D.

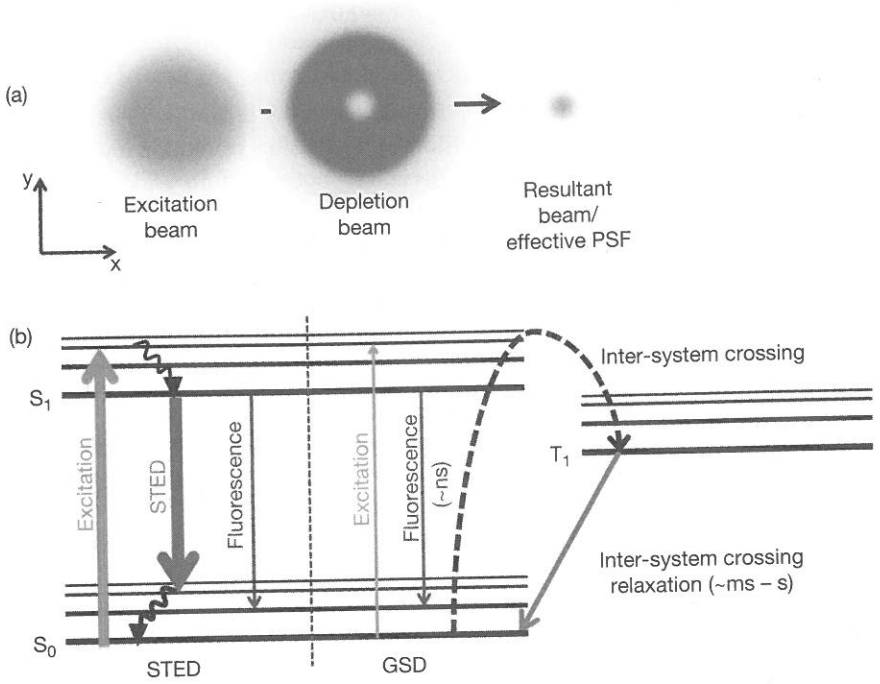

Figure 9.4 STED and GSD. (a) A 2D cross-section of the excitation, depletion, and resultant beams used in STED microscopy. The doughnut shape of the depletion beam can be achieved by placing a phase mask in the light path. (b) Jablonski diagram depicting STED and GSD. In STED, the depletion beam (labeled STED) de-populates the excited state (S_1). Fluorescence from very few fluorophores, which still remain in the excited state, is then recorded. In contrast, GSD works by "optical shelving." The electronic ground state (S_0) of fluorophores is depleted by pumping electrons into either the first triplet state (T_1) or other dark states. Electronic relaxations from these dark states occur at durations that are several orders of magnitude higher than that of fluorescence. At any given time, the ground state is thus sparsely populated, allowing only a few fluorophores to get excited.

As in STED, GSD requires reversible switching between on- and off-states of the fluorophore. However, one of the major differences between the two methods lies in the nature of the off-state. Rather than by stimulated depletion, the off-state in GSD is induced via ground state depletion through increasing the triplet state population (Figure 9.4b). Another difference between the two RESOLFT techniques is the use of a single continuous-wave laser for both excitation and depletion in GSD. A lateral resolution of ~50 nm has been demonstrated by applying GSD to the imaging of microtubules (114, 115) and to aggregates of SNAP-25 (114) or integrin-β proteins (115) in fixed cells.

SPEM/SSIM is a wide-field super-resolution technique that excites a fluorescent sample by structured or patterned illumination (116, 117). This way, unresolved information is first visible in the form of low-resolution moiré fringes, which are then computationally processed to obtain the final high-resolution image. Similar to other RESOLFT techniques, SSIM relies on the nonlinear relationship between the fluorescence emission rate and excitation intensity, and the practical resolving power is

determined by the SNR. The improvement in resolution is, however, only twofold over that obtained by conventional fluorescence microscopy, which is almost an order of magnitude less than that obtained by STORM/PALM/F-PALM. Nevertheless, SIM is currently the only subdiffraction high-resolution imaging technique that can produce multicolor 3D images of whole cells with enhancement of resolution in both lateral and axial directions while using conventional fluorescent probes and low intensity light sources. Upon implementing 3D-SIM to visualize interphase chromatin architecture and nuclear pore complex structure in formaldehyde-fixed cells, never-before seen details of these macromolecular structures were unraveled in their native nuclear milieu (120). In another report, Kner et al. (121) used a combination of speckle microscopy and SIM to observe the evolution of microtubules in living cultured cells with ~100-nm lateral resolution and ~100-ms time resolution. Recently, impressive time-lapsed 3D images of zebrafish and *Drosophila* embryos undergoing development were recorded using SIM based on a tunable light sheet, taking the potential of SIM to new heights (122). By utilizing multiple fluorescent tags and imaging embryos at multiple angles the group was able to generate a "digital" fly embryo, highlighting the morphological changes of the entire embryo as it develops.

The theoretical resolution limit of RESOLFT techniques can be described by an extension of Abbe's law:

$$\Delta d = \frac{\lambda}{2n\sin\alpha\sqrt{1+\left(\frac{I_{max}}{I_s}\right)}} \tag{6}$$

where I_{max} is the intensity of light bordering the center and I_s is the saturation intensity required to outperform competing spectroscopic transitions (123). When $I_{max}/I_s \rightarrow \infty$, in theory "infinite" resolution can be achieved (i.e., down to a single molecule or even smaller), but this comes at the cost of using very high-intensity beams that might damage sensitive samples like living cells. Due to this risk, RESOLFT is still generally implemented as an ensemble imaging technique, although single molecule detection is definitely possible (124).

CONCLUSIONS

The gap in attainable limits of resolution between traditional microscopy and electron microscopy (EM) has recently been bridged by the high-resolution imaging techniques discussed in this chapter. Ultra-high-resolution microscopy with conventional optics, which for a long time was thought to be the realm of EM, near-field imaging or negative refractive index superlenses (125), has now become commonplace. Importantly, the ultimate contribution that these optical techniques will have to science depends on their accessibility to researchers. To this end, several "out of the box" microscopes that implement PALM, SSIM, and STED have recently been commercialized by manufacturers like Zeiss and Leica. Additionally, user-friendly software packages, both commercial and open-source (such as ImageJ), have made it easier to implement these powerful techniques without the need for technical proficiency or prior experience.

SMFM techniques are mainly limited by the number of observables accessible per experiment, imposing the need to perform multiple assays to study complex biological processes. The future of SMFM lies in the ability to combine multiple tools into one adaptive instrument, such that the wealth of information obtained from a single sample is broadened. Techniques like 3D correlated EM (126), which combines the technical prowess of EM with the noninvasive nature of fluorescence microscopy, and SPT/single molecule FRET (127), have emerged as powerful tools to study the spatiotemporal evolution of molecules during various stages of cellular processes at very high resolution. The latter method can particularly probe conformational changes of proteins as they diffuse inside living cells.

Realizing the true potential of any technique relies on understanding its scope and limitations. However, factors considered as a bane in certain methods can be a boon in others. For instance, reactive oxygen species produced by fluorescent probes, which are considered to be toxic to living cells, can be used to oxidize certain contrast-enhancing agents to improve image quality in EM (128). Even non-fluorescent chromophores like heme, which typically contribute to high background in intracellular fluorescence imaging, can be imaged by STED microscopy to provide unique details on subcellular super-structures (129). In this fashion, molecules can be visualized label-free in their native cellular environment without the need for fluorophore conjugation.

Chu and coworkers recently improved the precision of wide-field imaging of biological samples by a factor of two through correcting for microscope drift with active feedback control, reaching sub-nm accuracy and resolution (130, 131). At such resolutions, it should become possible to obtain structural information of single molecules, for instance the distance between two subunits of a protein, even at very low molecule abundance and without the need to cool the sample below ambient temperatures (as required for EM and X-ray diffraction). The near future of SMFM will involve the implementation of such image acquisition and processing algorithms to spatially resolve the complex biological processes that enable life. Spatial resolution is, however, just one side of the coin since sufficient temporal resolution is also necessary, and both types of resolution are typically inversely related. Reaching higher (sub-millisecond) temporal resolution during biological imaging is mainly impeded by hardware limitations (e.g., the maximal frame rate of the camera), limited photon collection at high frame rates, decreasing SNR, and fast diffusion of molecules inside the cell, which leads to image blurring. Stroboscopic imaging techniques, where laser excitation pulses are synchronized with the camera frame rate, have emerged as tools to address these limitations (132). Development of faster and more sensitive cameras may in the future enable higher resolution also during single-particle tracking based on simple optical and excitation schemes. Considering the large strides that SMFM has taken over the past two decades, one can easily envision that large-scale multiplexed imaging of biomolecules (e.g., proteins, DNA, RNA) at sub-nanometer and sub-millisecond spatiotemporal resolution within live cells or even animals will become possible within the next two decades.

REFERENCES

1. Lecuyer E, et al. (2007) Global analysis of mRNA localization reveals a prominent role in organizing cellular architecture and function. *Cell* 131:174–187.
2. Oleynikov Y, Singer RH (2003) Real-time visualization of ZBP1 association with beta-actin mRNA during transcription and localization. *Curr Biol* 13:199–207.
3. Montero Llopis P, et al. (2010) Spatial organization of the flow of genetic information in bacteria. *Nature* 466:77–81.
4. Fusco D, et al. (2003) Single mRNA molecules demonstrate probabilistic movement in living mammalian cells. *Curr Biol* 13:161–167.
5. Schuler B, Lipman EA, Eaton WA (2002) Probing the free-energy surface for protein folding with single-molecule fluorescence spectroscopy. *Nature* 419:743–747.
6. Merchant KA, Best RB, Louis JM, Gopich IV, Eaton WA (2007) Characterizing the unfolded states of proteins using single-molecule FRET spectroscopy and molecular simulations. *Proc Natl Acad Sci USA* 104:1528–1533.
7. Ditzler MA, Rueda D, Mo J, Hakansson K, Walter NG (2008) A rugged free energy landscape separates multiple functional RNA folds throughout denaturation. *Nucleic Acids Res* 36:7088–7099.
8. Solomatin SV, Greenfeld M, Chu S, Herschlag D (2010) Multiple native states reveal persistent ruggedness of an RNA folding landscape. *Nature* 463:681–684.
9. Zhuang X, et al. (2002) Correlating structural dynamics and function in single ribozyme molecules. *Science* 296:1473–1476.
10. Rueda D, et al. (2004) Single-molecule enzymology of RNA: essential functional groups impact catalysis from a distance. *Proc Natl Acad Sci USA* 101:10066–10071.
11. Lipman EA, Schuler B, Bakajin O, Eaton WA (2003) Single-molecule measurement of protein folding kinetics. *Science* 301:1233–1235.
12. Ha T, et al. (1999) Single-molecule fluorescence spectroscopy of enzyme conformational dynamics and cleavage mechanism. *Proc Natl Acad Sci USA* 96:893–898.
13. Kaufman RJ (2000) Overview of vector design for mammalian gene expression. *Mol Biotechnol* 16:151–160.
14. Toprak E, Kural C, Selvin PR (2010) Super-accuracy and super-resolution getting around the diffraction limit. *Methods Enzymol* 475:1–26.
15. Greenleaf WJ, Woodside MT, Block SM (2007) High-resolution, single-molecule measurements of biomolecular motion. *Annu Rev Biophys Biomol Struct* 36:171–190.
16. Walter NG, Huang CY, Manzo AJ, Sobhy MA (2008) Do-it-yourself guide: how to use the modern single-molecule toolkit. *Nat Methods* 5:475–489.
17. Joo C, Balci H, Ishitsuka Y, Buranachai C, Ha T (2008) Advances in single-molecule fluorescence methods for molecular biology. *Ann Rev Biochem* 77:51–76.
18. Lewis A, et al. (2003) Near-field optics: from subwavelength illumination to nanometric shadowing. *Nat Biotechnol* 21:1378–1386.
19. Edidin M (2001) Near-field scanning optical microscopy, a siren call to biology. *Traffic* 2:797–803.
20. Axelrod D (1981) Cell-substrate contacts illuminated by total internal reflection fluorescence. *J Cell Biol* 89:141–145.
21. Tokunaga M, Imamoto N, Sakata-Sogawa K (2008) Highly inclined thin illumination enables clear single-molecule imaging in cells. *Nat Methods* 5:159–161.
22. Konopka CA, Bednarek SY (2008) Variable-angle epifluorescence microscopy: a new way to look at protein dynamics in the plant cell cortex. *Plant J* 53:186–196.

23. Nakano A (2002) Spinning-disk confocal microscopy—a cutting-edge tool for imaging of membrane traffic. *Cell Struct Funct* 27:349–355.
24. Rehemtulla A, Hamilton CA, Chinnaiyan AM, Dixit VM (1997) Ultraviolet radiation-induced apoptosis is mediated by activation of CD-95 (Fas/APO-1). *J Biol Chem* 272:25783–25786.
25. Gossen M, Bujard H (1992) Tight control of gene expression in mammalian cells by tetracycline-responsive promoters. *Proc Natl Acad Sci USA* 89:5547–5551.
26. Prescher JA, Bertozzi CR (2005) Chemistry in living systems. *Nat Chem Biol* 1:13–21.
27. Lord SJ, et al. (2008) A photoactivatable push-pull fluorophore for single-molecule imaging in live cells. *J Am Chem Soc* 130:9204–9205.
28. Lord SJ, et al. (2009) DCDHF fluorophores for single-molecule imaging in cells. *Chemphyschem* 10:55–65.
29. Davidson MW, Campbell RE (2009) Engineered fluorescent proteins: innovations and applications. *Nat Methods* 6:713–717.
30. Heilemann M, et al. (2008) Subdiffraction-resolution fluorescence imaging with conventional fluorescent probes. *Angew Chem Int Ed* 47:6172–6176.
31. Kapanidis AN, Weiss S (2002) Fluorescent probes and bioconjugation chemistries for single-molecule fluorescence analysis of biomolecules. *J Chem Phys* 117:10953–10964.
32. Dave R, Terry DS, Munro JB, Blanchard SC (2009) Mitigating unwanted photophysical processes for improved single-molecule fluorescence imaging. *Biophys J* 96:2371–2381.
33. Aitken CE, Marshall RA, Puglisi JD (2008) An oxygen scavenging system for improvement of dye stability in single-molecule fluorescence experiments. *Biophys J* 94:1826–1835.
34. Olenych SG, Claxton NS, Ottenberg GK, Davidson MW (2007) The fluorescent protein color palette. *Curr Protoc Cell Biol* 36: 21.5.1-21.5.34
35. Bogdanov AM, et al. (2009) Cell culture medium affects GFP photostability: a solution. *Nat Methods* 6:859–860.
36. Billinton N, Knight AW (2001) Seeing the wood through the trees: a review of techniques for distinguishing green fluorescent protein from endogenous autofluorescence. *Anal Biochem* 291:175–197.
37. Kredel S, et al. (2008) Optimized and far-red-emitting variants of fluorescent protein eqFP611. *Chem Biol* 15:224–233.
38. Magde D, Elson E, Webb WW (1972) Thermodynamic Fluctuations in a Reacting System—Measurement by Fluorescence Correlation Spectroscopy. *Phys Rev Lett* 29:705–708.
39. Poo M, Cone RA (1974) Lateral diffusion of rhodopsin in the photoreceptor membrane. *Nature* 247:438–441.
40. Gelles J, Schnapp BJ, Sheetz MP (1988) Tracking kinesin-driven movements with nanometre-scale precision. *Nature* 331:450–453.
41. De Brabander M, Nuydens R, Geuens G, Moeremans M, De Mey J (1986) The use of submicroscopic gold particles combined with video contrast enhancement as a simple molecular probe for the living cell. *Cell Motil Cytoskeleton* 6:105–113.
42. Geerts H, et al. (1987) Nanovid tracking: a new automatic method for the study of mobility in living cells based on colloidal gold and video microscopy. *Biophys J* 52:775–782.
43. Moerner WE, Kador L (1989) Optical detection and spectroscopy of single molecules in a solid. *Phys Rev Lett* 62:2535–2538.

44. Orrit M, Bernard J (1990) Single pentacene molecules detected by fluorescence excitation in a p-terphenyl crystal. *Phys Rev Lett* 65:2716–2719.
45. Ambrose WP, Basche T, Moerner WE (1991) Detection and Spectroscopy of Single Pentacene Molecules in a p- Terphenyl Crystal by Means of Fluorescence Excitation. *J Chem Phys* 95:7150–7163.
46. Van Oijen AM, Köhlera J, Schmidta J, Müllerb M, Brakenhoffb GJ (1998) 3-Dimensional super-resolution by spectrally selective imaging. *Chem Phys Lett* 292:183–187.
47. Yildiz A, et al. (2003) Myosin V walks hand-over-hand: single fluorophore imaging with 1.5-nm localization. *Science* 300:2061–2065.
48. Bobroff N (1986) Position measurement with a resolution and noise-limited instrument. *Rev Sci Instrum* 57:1152–1157.
49. Thompson RE, Larson DR, Webb WW (2002) Precise nanometer localization analysis for individual fluorescent probes. *Biophys J* 82:2775–2783.
50. Hua W, Chung J, Gelles J (2002) Distinguishing inchworm and hand-over-hand processive kinesin movement by neck rotation measurements. *Science* 295:844–848.
51. Forkey JN, Quinlan ME, Shaw MA, Corrie JE, Goldman (2003) Three-dimensional structural dynamics of myosin V by single-molecule fluorescence polarization. *Nature* 422:399–404.
52. Yildiz A, Tomishige M, Vale RD, Selvin PR (2004) Kinesin walks hand-over-hand. *Science* 303:676–678.
53. Gordon MP, Ha T, Selvin PR (2004) Single-molecule high-resolution imaging with photobleaching. *Proc Natl Acad Sci USA* 101:6462–6465.
54. Qu X, Wu D, Mets L, Scherer NF (2004) Nanometer-localized multiple single-molecule fluorescence microscopy. *Proc Natl Acad Sci USA* 101:11298–11303.
55. Das SK, Darshi M, Cheley S, Wallace MI, Bayley H (2007) Membrane protein stoichiometry determined from the step-wise photobleaching of dye-labelled subunits. *Chembiochem* 8:994–999.
56. Kuszak AJ, et al. (2009) Purification and functional reconstitution of monomeric mu-opioid receptors: allosteric modulation of agonist binding by Gi2. *J Biol Chem* 284:26732–26741.
57. Churchman LS, Okten Z, Rock RS, Dawson JF, Spudich JA (2005) Single molecule high-resolution colocalization of Cy3 and Cy5 attached to macromolecules measures intramolecular distances through time. *Proc Natl Acad Sci USA* 102:1419–1423.
58. Goshtasby A (1988) Image registration by local approximation methods. *Image and Vision Computing* 6:255–261.
59. Grunwald D, Singer RH (2010) In vivo imaging of labelled endogenous beta-actin mRNA during nucleocytoplasmic transport. *Nature* 467:604–607.
60. Kao HP, Verkman AS (1994) Tracking of single fluorescent particles in three dimensions: use of cylindrical optics to encode particle position. *Biophys J* 67:1291–1300.
61. Speidel M, Jonas A, Florin EL (2003) Three-dimensional tracking of fluorescent nanoparticles with subnanometer precision by use of off-focus imaging. *Opt Lett* 28:69–71.
62. Schütz GJ, et al. (2000) 3D imaging of individual ion channels in live cells at 40 nm resolution. *Single Molecules* 1:25–31.
63. Toprak E, Balci H, Blehm BH, Selvin PR (2007) Three-dimensional particle tracking via bifocal imaging. *Nano Lett* 7:2043–2045.

64. Yajima J, Mizutani K, Nishizaka T (2008) A torque component present in mitotic kinesin Eg5 revealed by three-dimensional tracking. *Nat Struct Mol Biol* 15:1119–1121.
65. Sun Y, McKenna JD, Murray JM, Ostap EM, Goldman YE (2009) Parallax: high accuracy three-dimensional single molecule tracking using split images. *Nano Lett* 9:2676–2682.
66. Sun Y, et al. (2010) Single-molecule stepping and structural dynamics of myosin X. *Nat Struct Mol Biol* 17:485–491.
67. Pavani SR, et al. (2009) Three-dimensional, single-molecule fluorescence imaging beyond the diffraction limit by using a double-helix point spread function. *Proc Natl Acad Sci USA* 106:2995–2999.
68. Thompson MA, Lew MD, Badieirostami M, Moerner WE (2010) Localizing and tracking single nanoscale emitters in three dimensions with high spatiotemporal resolution using a double-helix point spread function. *Nano Lett* 10:211–218.
69. Shannon CE (1949) Communication in the Presence of Noise. *Proceedings of the IRE* 37:10–21.
70. Ando R, Hama H, Yamamoto-Hino M, Mizuno H, Miyawaki A (2002) An optical marker based on the UV-induced green-to-red photoconversion of a fluorescent protein. *Proc Natl Acad Sci USA* 99:12651–12656.
71. Bates M, Blosser TR, Zhuang X (2005) Short-range spectroscopic ruler based on a single-molecule optical switch. *Phys Rev Lett* 94:108101.
72. Lukyanov KA, Chudakov D, Lukyanov S, Verkhusha V (2005) Photoactivatable fluorescent proteins. *Nat Rev Mol Cell Biol* 6:885–891.
73. Rust MJ, Bates M, Zhuang X (2006) Sub-diffraction-limit imaging by stochastic optical reconstruction microscopy (STORM). *Nat Methods* 3:793–795.
74. Betzig E, et al. (2006) Imaging intracellular fluorescent proteins at nanometer resolution. *Science* 313:1642–1645.
75. Hess ST, Girirajan TPK, Mason MD (2006) Ultra-high resolution imaging by fluorescence photoactivation localization microscopy. *Biophys J* 91:4258–4272.
76. Gould TJ, Verkhusha VV, Hess ST (2009) Imaging biological structures with fluorescence photoactivation localization microscopy. *Nat Protocols* 4:291–308.
77. Geisler C, et al. (2007) Resolution of lambda/10 in fluorescence microscopy using fast single molecule photo-switching. *Applied Phys A Mat Sci Proc* 88:223–226.
78. Egner A, et al. (2007) Fluorescence nanoscopy in whole cells by asynchronous localization of photoswitching emitters. *Biophys J* 93:3285–3290.
79. van de Linde S, Sauer M, Heilemann M (2008) Subdiffraction-resolution fluorescence imaging of proteins in the mitochondrial inner membrane with photoswitchable fluorophores. *J Struct Biol* 164:250–254.
80. Dempsey GT, et al. (2009) Photoswitching mechanism of cyanine dyes. *J Am Chem Soc* 131:18192–18193.
81. Heilemann M, van de Linde S, Mukherjee A, Sauer M (2009) Super-resolution imaging with small organic fluorophores. *Angew Chem Int Ed* 48:6903–6908.
82. Conley NR, Biteen JS, Moerner WE (2008) Cy3-Cy5 covalent heterodimers for single-molecule photoswitching. *J Phys Chem B* 112:11878–11880.
83. Osborn M, Webster RE, Weber K (1978) Individual microtubules viewed by immunofluorescence and electron microscopy in the same PtK2 cell. *J Cell Biol* 77:R27–34.
84. Adams SR, et al. (2002) New biarsenical ligands and tetracysteine motifs for protein labeling in vitro and in vivo: synthesis and biological applications. *J Am Chem Soc* 124:6063–6076.

85. Cao H, et al. (2007) A red cy3-based biarsenical fluorescent probe targeted to a complementary binding peptide. *J Am Chem Soc* 129:8672–8673.
86. Griffin BA, Adams SR, Tsien RW (1998) Specific covalent labeling of recombinant protein molecules inside live cells. *Science* 281:269–272.
87. Folling J, et al. (2007) Photochromic rhodamines provide nanoscopy with optical sectioning. *Angew Chem Int Ed* 46:6266–6270.
88. Andresen M, et al. (2007) Structural basis for reversible photoswitching in Dronpa. *Proc Natl Acad Sci USA* 104:13005–13009.
89. Shroff H, et al. (2007) Dual-color superresolution imaging of genetically expressed probes within individual adhesion complexes. *Proc Natl Acad Sci USA* 104:20308–20313.
90. Ando R, Flors C, Mizuno H, Hofkens J, Miyawaki A (2007) Highlighted generation of fluorescence signals using simultaneous two-color irradiation on Dronpa mutants. *Biophys J* 92:L97–99.
91. Stiel AC, et al. (2007) 1.8 A bright-state structure of the reversibly switchable fluorescent protein Dronpa guides the generation of fast switching variants. *Biochem J* 402:35–42.
92. Wiedenmann J, et al. (2004) EosFP, a fluorescent marker protein with UV-inducible green-to-red fluorescence conversion. *Proc Natl Acad Sci USA* 101:15905–15910.
93. Nienhaus K, Nienhaus GU, Wiedenmann J, Nar H (2005) Structural basis for photo-induced protein cleavage and green-to-red conversion of fluorescent protein EosFP. *Proc Natl Acad Sci USA* 102:9156–9159.
94. Fernández-Suárez M, Ting AY (2008) Fluorescent probes for super-resolution imaging in living cells. *Nat Rev Mol Cell Biol* 9:929–943.
95. Stiel AC, et al. (2008) Generation of monomeric reversibly switchable red fluorescent proteins for far-field fluorescence nanoscopy. *Biophys J* 95:2989–2997.
96. Andresen M, et al. (2008) Photoswitchable fluorescent proteins enable monochromatic multilabel imaging and dual color fluorescence nanoscopy. *Nat Biotechol* 26:1035–1040.
97. Huang B, Jones SA, Brandenburg B, Zhuang X (2008) Whole-cell 3D STORM reveals interactions between cellular structures with nanometer-scale resolution. *Nat Methods* 5:1047–1052.
98. Huang B, Wang W, Bates M, Zhuang X (2008) Three-dimensional super-resolution imaging by stochastic optical reconstruction microscopy. *Science* 319:810–813.
99. Juette MF, et al. (2008) Three-dimensional sub-100 nm resolution fluorescence microscopy of thick samples. *Nat Methods* 5:527–529.
100. Helmchen F, Denk W (2005) Deep tissue two-photon microscopy. *Nat Methods* 2:932–940.
101. Levi V, Ruan Q, Gratton E (2005) 3-D particle tracking in a two-photon microscope: application to the study of molecular dynamics in cells. *Biophys J* 88:2919–2928.
102. Levi V, Gratton E (2008) Chromatin dynamics during interphase explored by single-particle tracking. *Chromosome Res* 16:439–449.
103. Vaziri A, Tang J, Shroff H, Shank CV (2008) Multilayer three-dimensional super resolution imaging of thick biological samples. *Proc Natl Acad Sci USA* 105:20221–20226.
104. Shroff H, Galbraith CG, Galbraith JA, Betzig E (2008) Live-cell photoactivated localization microscopy of nanoscale adhesion dynamics. *Nat Methods* 5:417–423.

105. Biteen JS, Moerner WE (2010) Single-molecule and superresolution imaging in live bacteria cells. *Cold Spring Harb Perspect Biol* 2:a000448.
106. Biteen JS, et al. (2008) Super-resolution imaging in live Caulobacter crescentus cells using photoswitchable EYFP. *Nat Methods* 5:947–949.
107. Hess ST, et al. (2007) Dynamic clustered distribution of hemagglutinin resolved at 40 nm in living cell membranes discriminates between raft theories. *Proc Natl Acad Sci USA* 104:17370–17375.
108. Manley S, et al. (2008) High-density mapping of single-molecule trajectories with photoactivated localization microscopy. *Nat Methods* 5:155–157.
109. Tatavarty V, Kim E-J, Rodionov V, Yu J (2009) Investigating sub-spine actin dynamics in rat hippocampal neurons with super-resolution optical imaging. *PLoS ONE* 4:e7724.
110. Lang MC, Engelhardt J, Hell SW (2007) 4Pi microscopy with linear fluorescence excitation. *Opt Lett* 32:259–261.
111. Gustafsson MG, Agard DA, Sedat JW (1999) I5M: 3D widefield light microscopy with better than 100 nm axial resolution. *J Microscopy* 195:10–16.
112. Hell SW, Wichmann J (1994) Breaking the diffraction resolution limit by stimulated emission: stimulated-emission-depletion fluorescence microscopy. *Opt Lett* 19:780–782.
113. Dyba M, Jakobs S, Hell SW (2003) Immunofluorescence stimulated emission depletion microscopy. *Nat Biotechnol* 21:1303–1304.
114. Bretschneider S, Eggeling C, Hell SW (2007) Breaking the diffraction barrier in fluorescence microscopy by optical shelving. *Phys Rev Lett* 98:218103.
115. Folling J, et al. (2008) Fluorescence nanoscopy by ground-state depletion and single-molecule return. *Nat Methods* 5:943–945.
116. Heintzmann R, Jovin TM, Cremer C (2002) Saturated patterned excitation microscopy—a concept for optical resolution improvement. *J Opt Soc Am A Opt Image Sci Vis* 19:1599–1609.
117. Gustafsson MG (2005) Nonlinear structured-illumination microscopy: wide-field fluorescence imaging with theoretically unlimited resolution. *Proc Natl Acad Sci USA* 102:13081–13086.
118. Willig KI, et al. (2006) Nanoscale resolution in GFP-based microscopy. *Nat Methods* 3:721–723.
119. Schmidt R, et al. (2008) Spherical nanosized focal spot unravels the interior of cells. *Nat Methods* 5:539–544.
120. Schermelleh L, et al. (2008) Subdiffraction multicolor imaging of the nuclear periphery with 3D structured illumination microscopy. *Science* 320:1332–1336.
121. Kner P, Chhun BB, Griffis ER, Winoto L, Gustafsson MG (2009) Super-resolution video microscopy of live cells by structured illumination. *Nat Methods* 6:339–342.
122. Keller PJ, et al. (2010) Fast, high-contrast imaging of animal development with scanned light sheet-based structured-illumination microscopy. *Nat Methods* 7:637–642.
123. Hell SW (2007) Far-field optical nanoscopy. *Science* 316:1153–1158.
124. Kasper R, et al. (2010) Single-molecule STED microscopy with photostable organic fluorophores. *Small* 6:1379–1384.
125. Smolyaninov, II, Hung YJ, Davis CC (2007) Magnifying superlens in the visible frequency range. *Science* 315:1699–1701.

126. Sun MG, et al. (2007) Correlated three-dimensional light and electron microscopy reveals transformation of mitochondria during apoptosis. *Nat Cell Biol* 9:1057–1065.
127. Sakon JJ, Weninger KR (2010) Detecting the conformation of individual proteins in live cells. *Nat Methods* 7:203–205.
128. Meisslitzer-Ruppitsch C, Rohrl C, Neumuller J, Pavelka M, Ellinger A (2009) Photooxidation technology for correlated light and electron microscopy. *J Microscopy* 235:322–335.
129. Min W, et al. (2009) Imaging chromophores with undetectable fluorescence by stimulated emission microscopy. *Nature* 461:1105–1109.
130. Pertsinidis A, Zhang Y, Chu S (2010) Subnanometre single-molecule localization, registration and distance measurements. *Nature* 466:647–651.
131. Mortensen KI, Churchman LS, Spudich JA, Flyvbjerg H (2010) Optimized localization analysis for single-molecule tracking and super-resolution microscopy. *Nat Methods* 7:377–381.
132. Elf J, Li GW, Xie XS (2007) Probing transcription factor dynamics at the single-molecule level in a living cell. *Science* 316:1191–1194.
133. Heuser J (1980) Three-dimensional visualization of coated vesicle formation in fibroblasts. *J Cell Biol* 84:560–583.